Available online at www.sciencedirect.com
ScienceDirect
Journal of Power Sources 159 (2006) 514–523
JOURNAL OF POWER SOURCES
www.elsevier.com/locate/jpowsour

Dynamic analysis of gas transport in cathode side of PEM fuel cell with interdigitated flow field

Jiang Zou [a], Xiao-Feng Peng [a], Wei-Mon Yan [b,*]

[a] *Laboratory of Phase Change and Interfacial Transport Phenomena, Department of Thermal Engineering, Tsinghua University, Beijing 100084, China*
[b] *Department of Mechatronic Engineering, Huafan University, Shih-Ting, Taipei 223, Taiwan*

Received 21 September 2005; received in revised form 25 October 2005; accepted 4 November 2005
Available online 15 December 2005

Abstract

The dynamic performance of PEM fuel cell is one of the most important criteria in its design with application to mobile systems and portable devices. To analyze the features, this work employs an unsteady model about single phase transport in cathode side of PEM fuel cell with interdigitated flow field, which considers both convection and diffusion processes. Two types of dynamic performances, start-up and state-to-state operations, are analyzed. The effects of channel width fraction, porosity of the gas diffusion layer, pressure drop and the surface overpotential of the catalyst layer on the dynamic performance are investigated in detail. Predicted results found that the response time is generally quite fast, less than 0.1 s, to reach the 90% response. The time interval from the start-up to a steady state or from one steady state to another steady state mainly depends on the end condition.

Keywords: PEM fuel cell; Dynamic response; Gas transport; Interdigitated flow field

1. Introduction

Proton exchange membrane (PEM) fuel cells have extensive applications due to their merits of high efficiency, low pollutant emission and convenience, and now the main application is as power generators of mobile systems. Moreover, it also has some promising applications in portable devices, such as mobile phones, laptop computers and digital cameras. In applications of PEM fuel cells to these systems, the dynamic response of the system is important. The dynamic response involves two operations, start-up operation and state-to-state operation. The time interval from the start to a steady state or from one steady state to another steady state is one of the significant performance characteristics of the system. The dynamic response of the fuel cell mainly depends on operating conditions, mass transport process in the cells, electrochemical reaction kinetics, mechanical design and manufacturing process, etc. Among these factors, the reactant gas transport in the cell is one of the crucial points.

The gas diffusion layer (GDL) morphology, geometry and porosity, as well as the flow channel arrangement, e.g., parallel, serpentine or interdigitated channel, gas pressure drop have significant influences on the optimization of the cell performance. Some studies on modeling mass transport and parametric analysis in the PEM fuel cell have been performed. The pioneer work is from Bernardi and Verbrugge [1], who developed a one-dimensional isothermal model to examine mass transport in fuel cell. Gurau et al. [2] proposed a one-dimensional model to examine the characteristics of the mass transport of reactant gas in a half-cell, in which the effects of the porosity and the tortuosity of GDL and the catalyst layer were investigated. Springer et al. [3] predicted the net water-per-proton flux ratio across the membrane. Okada and colleagues [4] studied water transport with and without impurity ions in membranes of PEM fuel cells. For more details of the steady-state flow distribution and gas diffusion, a number of studies on two and three dimensional transport phenomena in PEM fuel cells have been carried out. Dutta et al. [5] used the software package to analyze the distributions of gas

* Corresponding author. Tel.: +886 2 2663 2102; fax: +886 2 2663 2143.
E-mail address: wmyan@huafan.hfu.edu.tw (W.-M. Yan).

0378-7753/$ – see front matter © 2005 Elsevier B.V. All rights reserved.
doi:10.1016/j.jpowsour.2005.11.018

Nomenclature

D	mass diffusivity, $m^2\ s^{-1}$
D^e	effective mass diffusivity, $m^2\ s^{-1}$
F	Faraday constant, 96487 C mol^{-1}
j	transfer current density, Am^{-2}
i	average current density, Am^{-2}
k	permeability, m^2
l_c	length of channel, m
l_s	length of shoulder, m
M_{O_2}	molecular mass of oxygen, 32.0 kg $kmol^{-1}$
M_{H_2O}	molecular mass of oxygen, 18.0 kg $kmol^{-1}$
n	number of electrons in relation participating
P	pressure, Pa
R	universal gas constant, 8.314 J $mol^{-1}\ K^{-1}$
R_h	hydaulic radius, m
S_c	thickness of catalyst layer, m
S_d	thickness of gas diffusion layer, m
S_m	thickness of membrane, m
t	time, s
t_c	time constant
T	temperature, K
v_x	superficial velocity in x direction
v_y	superficial velocity in y direction
V	cell voltage
V_{oc}	ideal cell potential, V
w_{O_2}	mass fraction of oxygen
w_{H_2O}	mass fraction of water vapor
x	x direction
y	y direction

Greek letters

ε_1	porosity of GDL
ε_2	porosity of catalyst layer
η	surface overpotential, V
λ	channel width fraction, l_c/l_s
λ_w	membrane water content
μ	Viscosity
κ	reaction rate constant, mol $m^{-3}\ s^{-1}$
ρ	density, Kg m^{-3}
σ	ionic conductivity of the ionomer, $\Omega^{-1}\ m^{-1}$
τ	tortuosity
Φ	ionomer phase potential, V

density and velocity in flow channel and GDL. Jordan et al. [6] examined the influence of diffusion-layer morphology on cell performance. A model of the hydrophobilicity and the porosity of the gas-diffusion layer was used to explain the influence of the diffusion-layer morphology. Yi and Nguyen [7] developed a two-dimension model to examine the multi-component gas transport in PEM fuel cells of interdigitated flow channel. And then they [8] developed a two-phase model to examine the water and thermal management of PEM fuel cells with interdigitated flow field. They found that the interdigitated gas distributors can reduce mass-transport overpotential and improve the flooding phenomena in the cathode side. Yan et al. [9] developed a two-dimensional model to investigate gas reactant transport at various conditions of flow channel width ratio (λ = channel width l_c/shoulder width l_s) and GDL porosity ε_1. They disclosed that an increase in either λ or ε_1 may lead to a better cell performance. At the case with a relatively low overpotential, better uniformity in current density distribution along the width of the cell can be attained. Chen et al. [10] investigated the transient behavior of the water transport across the membrane of the PEM fuel cell to seek for effective control schemes so that the best dynamic performance of the fuel cell can be obtained. It is found that both a larger starting operational current density and a smaller operational current density can lead to a shorter dynamic response time, while control of the humidification of the fed fuel is the most powerful as well as the most feasible scheme. Yan et al. [11] studied transient gas transport in the cathode side of PEM fuel cell with straight flow field. They concluded that an increase in channel width ratioλ, or surface overpotential η may lead to a faster dynamic response of a PEM fuel cell subjected a start-up operation, and a higher surface overpotential results in a fuel cell with a faster surface reaction rate. The time interval from start-up to a steady state may be as long as 10 s due to the mass transport lag, but it is only about 0.4 s to reach the 90% response. The surface overpotential η represents the voltage loss due to chemical reaction within the catalyst layer, and is the effect of the current of a fuel cell. A higher surface overpotential means a faster surface reaction rate when other conditions are the same. For a certain fuel cell system, the value of η or the reaction rate can be controlled by adjusting external load.

Although the previous studies concern many issues about the PEM fuel cells, from steady state analysis to unsteady analysis, no work has been done about dynamic analysis of fuel cell with interdigitated flow field. It features the combined influences of convection and diffusion processes and excellent anti-flooding function. The objective of this work is to numerically investigate the dynamical response of this type of PEM fuel cells. Parametric analysis is performed. The emphasis of the analysis is placed on the influences of the channel width ratio λ, the porosity of the GDL ε_1 and pressure drop ΔP on fuel cell. By applying the time-dependent mass transport model developed in this work, the effects of these parameters and the surface overpotential η on the transient characteristics of the mass transport and the dynamic response of the cell performance are explored.

2. Numerical modeling

2.1. Problem statement

In this work, the single phase multi-component transport process is considered only. This assumption has its limitation. The maximum vapor pressure in the cell is limited to be below the saturated pressure at the operating temperature, which is 0.047 MPa at 80 °C. And generally, the value of the maximum vapor pressure increases with current density when it is below the saturated pressure. Therefore, the density current can not be too large.

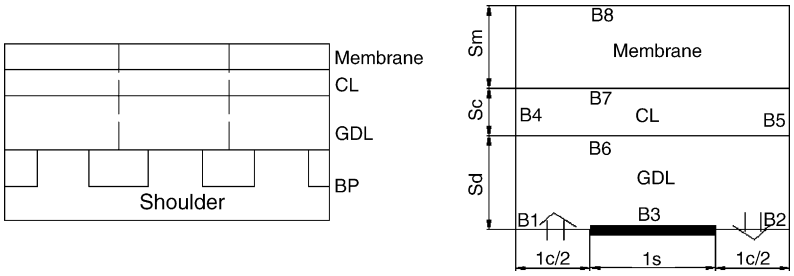

Fig. 1. Half-cell model of a PEM fuel cell. BP: bipolar plate; GDL: gas diffusion layer; CL: catalyst layer; l_c: width of the channel; l_s: width of the shoulder.

Otherwise, the result will not reflect the real flow process. Wang et al. [12] predicted the onset current density for the two-phase regime at different inlet dry air velocity under certain configuration. When the velocity is about $1\,\mathrm{m\,s^{-1}}$, the critical current density is about $2\,\mathrm{A\,cm^{-2}}$. Although single phase condition is not correct at the operating condition of high current density, it is often reasonable in low current density with dry air entry when no liquid water is formed or the liquid saturation is very low.

Multicomponent consideration accounts for the effects of such inert species as nitrogen and water vapor. Two-dimensional condition is assumed, and the computational domain is perpendicular to the axial direction of channels in bipolar plate. This treatment is consistent with the main mass transport direction normal to the channels in the fuel cell. As shown in Fig. 1, only half-cell is adopted. Gas mixture enters the gas diffusion layer (GDL) from channels connected with inlet plenum of bipolar plate and exits from its neighbor channels. For simplicity, a unit structure is considered as the computational domain, as shown in the right graph. There are totally three layers, gas diffusion layer (GDL), catalyst layer (CL) and membrane. Gas transports within the GDL and CL, and convection and diffusion processes are both crucial in this problem, which is different from the gas transport in the PEM fuel cell with other types of flow fields.

2.2. Assumption

In this study, the membrane, GDL, and CL are respectively treated as homogeneous porous media with uniform morphological properties, such as porosity, tortuosity and permeability. The gas mixture is considered to be ideal gas and the viscosity is assumed constant. Isothermal condition is assumed, so energy equation can be omitted.

Gravity effect is neglected. Darcy's law is employed to account for superficial velocity in porous medium. Fickian law is introduced to account for species diffusion process. The oxygen reduction reaction (ORR) is adopted in the analysis.

2.3. Mathematical model

The single phase multicomponent model of PEMFC consists of four kinds of principle equations: continuity, momentum, species and phase potential equations.

2.3.1. Continuity equation

$$-\frac{\partial(\rho v_x)}{\partial x}-\frac{\partial(\rho v_y)}{\partial y}=\frac{j}{2nF}(M_{\mathrm{O_2}}2M_{\mathrm{H_2O}})+\varepsilon\frac{\partial\rho}{\partial t}. \tag{1}$$

Where ε represents the porosity of GDL ε_1 or CL ε_2, and j represents the cathode transfer volumetric current density and can be formulated by the following equation according to the ORR assumption.

$$j=\begin{cases} nF\kappa w_{\mathrm{O_2}}\exp\left(\dfrac{\alpha nF}{RT}\eta\right) & \text{in the catalyst layer}\\ 0 & \text{in the GDL}\end{cases} \tag{2}$$

2.3.2. Momentum equation

According to Darcy's law, superficial velocity in porous media is expressed as below.

$$v_x=-\frac{k}{\mu}\frac{\partial P}{\partial x}. \tag{3a}$$

$$v_y=-\frac{k}{\mu}\frac{\partial P}{\partial y}. \tag{3b}$$

In Eqs. (3), the k is permeability of porous media. To test the influence of porosity of GDL on mass transfer, especially convection process, Carman-Kozeny equation [13] is employed to express the permeability k as a function of porosity ε and hydraulic radius R_h.

$$k=\frac{\varepsilon R_{\mathrm{h}}^2}{f} \tag{4}$$

where the f is the Kozeny constant. It is assumed that the morphology of the same kind of porous media keeps similar when its porosity changes, and

$$R_{\mathrm{h}}=C\sqrt{\varepsilon} \tag{5}$$

So the relation between permeability and porosity is established as below

$$k=\frac{\varepsilon^2}{f'},\quad \text{where } f'=\frac{f}{C} \tag{6}$$

In this work, the value of f' is set to be $3\times10^{11}\,\mathrm{m^{-2}}$. When the value of ε is 0.6, the corresponding permeability is $1.2\times10^{-12}\,\mathrm{m^2}$.

2.3.3. Species equation

Only two kinds of species equations are needed, and here oxygen and water vapor are selected.

$$\frac{\partial}{\partial x}\left(\rho D^{e}_{O_2}\frac{\partial w_{O_2}}{\partial x}\right)+\frac{\partial}{\partial y}\left(\rho D^{e}_{O_2}\frac{\partial w_{O_2}}{\partial y}\right)-\frac{\partial}{\partial x}(\rho w_{O_2}v_x)-\frac{\partial}{\partial y}(\rho w_{O_2}v_y)=\frac{j}{2nF}M_{O_2}+\varepsilon\frac{\partial(\rho w_{O_2})}{\partial t} \tag{7}$$

$$\frac{\partial}{\partial x}\left(\rho D^{e}_{H_2O}\frac{\partial w_{H_2O}}{\partial x}\right)+\frac{\partial}{\partial y}(\rho D^{e}_{H_2O}\frac{\partial w_{H_2O}}{\partial y})-\frac{\partial}{\partial x}(\rho w_{H_2O}v_x)-\frac{\partial}{\partial y}(\rho w_{H_2O}v_y)=\varepsilon\frac{\partial(\rho w_{H_2O})}{\partial t}-\frac{j}{nF}M_{H_2O} \tag{8}$$

Combining Eqs. (1), (3), (7) and (8) yields

$$\frac{\partial}{\partial x}\left(\rho D^{e}_{O_2}\frac{\partial w_{O_2}}{\partial x}\right)+\frac{\partial}{\partial y}\left(\rho D^{e}_{O_2}\frac{\partial w_{O_2}}{\partial y}\right)+\frac{k}{\mu}\frac{\partial w_{O_2}}{\partial x}\left(\rho\frac{\partial P}{\partial x}\right)+\frac{k}{\mu}\frac{\partial w_{O_2}}{\partial y}\left(\rho\frac{\partial P}{\partial y}\right)=\frac{j}{2nF}(M_{O_2}(1-w_{O_2})+2w_{H_2O}M_{H_2O})+\rho\varepsilon\frac{\partial w_{O_2}}{\partial t} \tag{9}$$

$$\frac{\partial}{\partial x}\left(\rho D^{e}_{H_2O}\frac{\partial w_{H_2O}}{\partial x}\right)+\frac{\partial}{\partial y}\left(\rho D^{e}_{H_2O}\frac{\partial w_{H_2O}}{\partial y}\right)+\frac{k}{\mu}\frac{\partial w_{H_2O}}{\partial x}\left(\rho\frac{\partial P}{\partial x}\right)+\frac{k}{\mu}\frac{\partial w_{H_2O}}{\partial y}\left(\rho\frac{\partial P}{\partial y}\right)=\frac{j}{2nF}(-M_{O_2}w_{H_2O}+2w_{H_2O}M_{H_2O}-2M_{H_2O})+\rho\varepsilon\frac{\partial w_{H_2O}}{\partial t} \tag{10}$$

The effective diffusivities of oxygen and water vapor are as below.

$$D^{e}_{O_2}=D_{O_2}\varepsilon^{\tau} \tag{11a}$$

$$D^{e}_{H_2O}=D_{H_2O}\varepsilon^{\tau} \tag{11b}$$

2.3.4. Phase potential equations

$$\frac{\partial}{\partial x}\left(\sigma\frac{\partial\Phi}{\partial x}\right)+\frac{\partial}{\partial y}\left(\sigma\frac{\partial\Phi}{\partial y}\right)=0\text{ in the membrane} \tag{12}$$

$$\frac{\partial}{\partial x}\left(\varepsilon^{\tau}\sigma\frac{\partial\Phi}{\partial x}\right)+\frac{\partial}{\partial y}\left(\sigma\varepsilon^{\tau}\frac{\partial\Phi}{\partial y}\right)=j\text{ in the catalyst layer,} \tag{13}$$

In the above equations, the Φ is ionomer phase potential and σ is the membrane ionic conductivity and is evaluated by

$$\sigma=(0.5139\lambda_w-0.326)\times\exp\left[1268\times\left(\frac{1}{303}-\frac{1}{T}\right)\right] \tag{14}$$

2.3.5. Boundary and initial conditions

For description simplicity, each boundary is numbered in Fig. 1, from B1 to B8. At boundary B1,

$$P=P_{in},\quad w_{O_2}=w_{O_2in},\quad w_{H_2O}=w_{H_2O,in} \tag{15a}$$

In this work, w_{O_2in}, w_{H_2Oin} are respectively set 0.17 and 0.01. At boundary B2,

$$P=P_{out},\quad \frac{\partial w_{O_2}}{\partial n}=0,\quad \frac{\partial w_{H_2O}}{\partial n}=0 \tag{15b}$$

Here P_{out} is set 0.1 MPa.

At boundary B7, total mass flux is

$$\frac{k}{\mu}\rho\frac{\partial P}{\partial y}=2S_c\alpha'\frac{j}{nF}M_{H_2O} \tag{15c}$$

where α' represents the net water transport coefficient in the membrane, and is mainly combined effect of electro-osmotic drag and diffusion. The value of α' depends on several conditions, such as type and thickness of membrane, water content of membrane, and have a quite wide range [14,15]. For certain conditions, the value of α' can be assumed constant, and is specified to be 0.5 in this work according to related stusdies [7,16].

Oxygen and water vapor flux are respectively

$$\left(\rho D^{e}_{O_2}\frac{\partial w_{O_2}}{\partial y}+w_{O_2}\frac{k}{\mu}\rho\frac{\partial P}{\partial y}\right)\Bigg|_{B7}=0 \tag{15d}$$

$$\left(\rho D^{e}_{H_2O}\frac{\partial w_{H_2O}}{\partial y}+w_{H_2O}\frac{k}{\mu}\rho\frac{\partial P}{\partial y}\right)\Bigg|_{B7}=2S_c\alpha'\frac{j}{nF}M_{H_2O} \tag{15e}$$

where S_c is height of the catalyst layer. Here there is an assumption that electrical conduction is one-dimensional and oxygen concentration at the interface represents average value in the catalyst layer.

Combining Eqs. (15c)–(15e), we have the reduced expression for the condition of boundary B7

$$\frac{\partial P}{\partial n}\Bigg|_{B7}=\frac{2S_c\alpha'(j/nF)M_{H_2O}}{(k/m)\rho} \tag{15f}$$

$$\frac{\partial w_{O_2}}{\partial n}\Bigg|_{B7}=\frac{-2w_{O_2}S_c\alpha'(j/nF)M_{H_2O}}{\rho D^{e}_{O_2}} \tag{15g}$$

$$\frac{\partial w_{H_2O}}{\partial n}\Bigg|_{B7}=\frac{(1-w_{H_2O})2S_c\alpha'(j/nF)M_{H_2O}}{\rho D^{e}_{H_2O}} \tag{15h}$$

At boundary B6,

$$\left(\rho D^{e}_{O_2}\frac{\partial w_{O_2}}{\partial n}\right)\Bigg|_{+}=\left(\rho D^{e}_{O_2}\frac{\partial w_{O_2}}{\partial n}\right)\Bigg|_{-} \tag{15i}$$

$$\left(\rho D^{e}_{H_2O}\frac{\partial w_{H_2O}}{\partial n}\right)\Bigg|_{+}=\left(\rho D^{e}_{H_2O}\frac{\partial w_{H_2O}}{\partial n}\right)\Bigg|_{-} \tag{15j}$$

$$\left(\frac{k}{\mu}\frac{\partial P}{\partial n}\right)\Bigg|_{+}\left(\frac{k}{\mu}\frac{\partial P}{\partial n}\right)\Bigg|_{-} \tag{15k}$$

The boundary conditions for phase potential Φ are as follows. At boundaries B4 and B5

$$\frac{\partial \Phi}{\partial x} = 0 \tag{16a}$$

At boundary B7

$$\Phi_+ = \Phi_-, \tag{16b}$$

$$\varepsilon^{\tau} \frac{\partial \Phi}{\partial y}\bigg|_- = \frac{\partial \Phi}{\partial y}\bigg|_+ . \tag{16c}$$

At boundary B6

$$\frac{\partial \Phi}{\partial y} = 0 \tag{16d}$$

At boundary B8

$$\Phi = 0 \tag{16e}$$

There are two types of initial condition. For start-up operation, the initial condition is as below.

$$w_{O_2} = 0.0, \quad w_{H_2O} = 0.0 \tag{17}$$

And for state-to-state operation, the initial condition is the gas distribution of the former steady state.

The cell potential V is evaluated by subtracting surface overpotential η and the average phase potential difference $\Delta\Phi$ between boundary B8 and boundary B7 from the ideal cell potential V_{OC}, that is,

$$V = V_{OC} - \eta - \Delta\Phi. \tag{18}$$

3. Numerical method

To numerically solve the above set of equations, the implicit finite difference method is adopted. The time derivative term is approximated by the implicit or backward difference scheme, and space derivative term by the central difference scheme. With the coupled finite-difference equations, the linear algebraic equations are solved simultaneously, firstly obtaining approximate pressure and velocity profile by solving continuity and momentum equations and then calculating species profile by species equations. The uniform grid system is used in this study. The grid points in the x and y directions are 81×316, respectively, which is tested to satisfy the grid independent requirement.

4. Results and discussion

Four important parameters are chosen to investigate their effects on the performance of the PEM fuel cells. They are channel width fraction $\lambda \equiv l_c/l_s$, the porosity of GDL ε_1, pressure drop ΔP and surface overpotential η. The values of other parameters considered in the present study, listed in Table 1, are derived from the practical applications. For the PEM fuel cell with straight flow field, channel width fraction λ affects the cell performance significantly, and an increase in λ may lead to a better cell performance [9,11]. In this work, however, the results show that λ just slightly influences the cell performance. The different transport process and boundary conditions may lead to this result. For the PEM fuel cell with straight flow field, only diffusion process accounts for gas transport and oxygen mass fraction w_{O_2} at the exit is considered to be constant. While for the PEM fuel cell with interdigitated flow field, the convection and the diffusion processes are combined and the normal gradient of w_{O_2} at the exit is zero. So, this paper will not analyze the effect of λ further on the cell performance, and the default value of λ is fixed. The results are organized in two sections, start-up operation and state-to-state operation.

Just as Yan et al. [11] indicated, although it may spend considerably long time to reach completely a steady state due to the mass transport lag, it needs only quite little time to approach 90% response. So, it is necessary to define a time constant t_c that

Table 1
The values of the parameters used in this work

Physical quantity	Notation	Unit	Value	Reference
Viscosity of gas	μ_g	kg m^{-1} s	2.03×10^{-5}	[17]
O2 diffusivity with substance of Air[a]	D_{O_2}	m^2 s^{-1}	2.71×10^{-5}	Incropera and DeWitt, p.927 [18]
H_2O diffusivity with substance of Air[a]	D_{H_2}	m^2 s^{-1}	3.35×10^{-5}	Incropera and DeWitt, p.927 [18]
Absolute Permeability in CL	k_{CL}	m^2	1.2×10^{-15}	[17]
Porosity of CL	ε_{CL}		0.4	[17]
Reaction rate constant	κ	kmol m^{-3} s	1.5×10^{-5}	[11]
Tortuosity of GDL/CL	τ		1.5	[11]
Net water transport coefficient of the membrane	α'		0.5	Set
Universal gas constant	R	J kmol^{-1} K^{-1}	8314	Constant
Faraday constant	F	c kmol^{-1}	96487000	Constant
Operation temperature	T	K	353	Set
Transfer coefficient for the reaction	α		1	Set
Number of electrons in relation participating	n		2	Constant
Thickness of GDL	S_d	m	3.0×10^{-4}	Set
Thickness of CL	S_c	m	1.5×10^{-5}	Set
Thickness of membrane	S_m	m	2.0×10^{-4}	Set
Width of channel	l_c	m	1.0×10^{-3}	Set
Width of shoulder	l_s	m	1.0×10^{-3}	Set

[a] The values are derived at the pressure 1 atm and temperature 353 K.

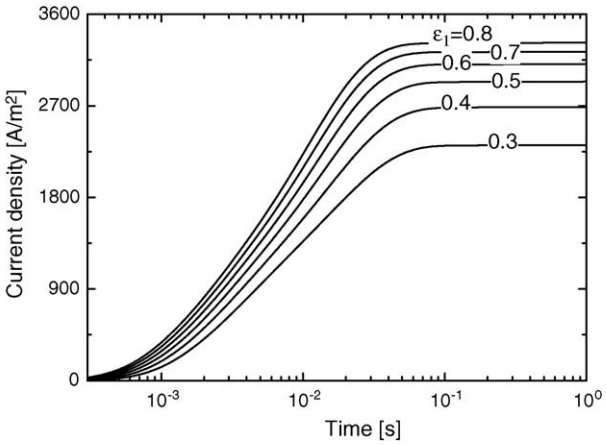

Fig. 2. Effects of GDL porosity ε_1 on time evolution of average current density when the PEM fuel cell is subjected to a start-up operation at $\Delta P = 7$ mbar, $\eta = 0.2$ V.

reflects how long a start-up operation or a state-to-state operation will almost reach. In the present study, the time constant is defined as the time interval needed to reach 90% response of average current density. For the start-up operation,

$$i(t_c) = 0.9i(t = \infty) \tag{19a}$$

For the state-to-state condition,

$$i(t_c) = 0.1i_1 + 0.9i_2 \tag{19b}$$

Where i_1, i_2 are respectively, the average current density of the former steady state and the latter steady state. Start-up operation can be considered as a special case of state-to-state operation when i_1 is zero.

4.1. Start-up operation

In start-up operation, the initial current density is zero as initial oxygen mass fraction in catalyst layer is zero. After the system is started up, oxygen mass fraction and current density gradually rise, and soon approach a certain condition. The system is regarded to reach a steady state when it satisfies a certain criteria.

Fig. 2 denotes the effects of GDL porosity ε_1 on the time evolution of average current density when the PEM fuel cell is subjected to a start-up operation under the condition of pressure drop 7 mbar and surface overpotential 0.2 V. It is clear that as the ε_1 increases, the average current density in steady state rises. This means that better mass transport in the PEM fuel cell is noticed for a larger GDL porosity. In addition, the response time of start-up operation is fast for a larger GDL porosity. So, a

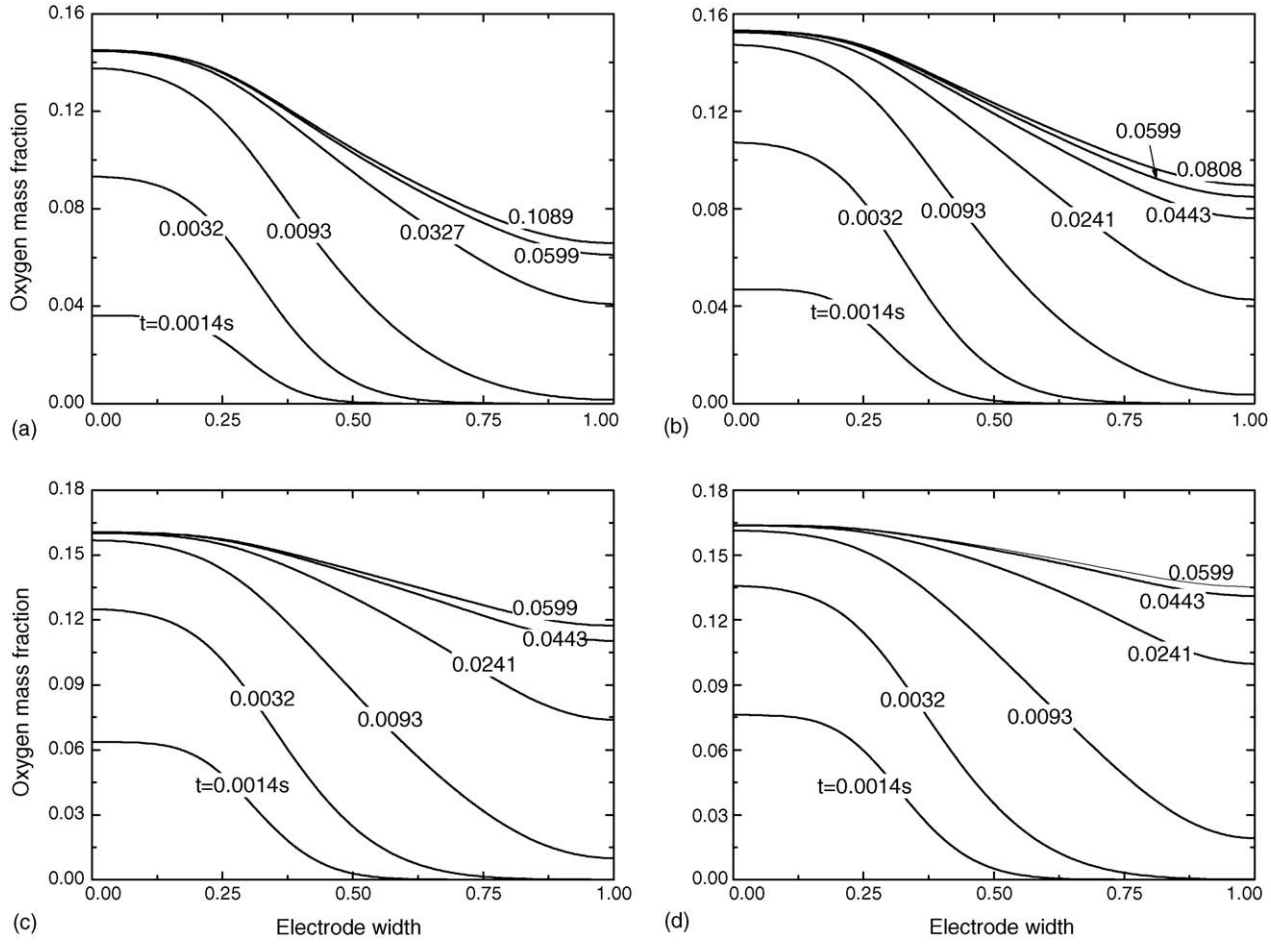

Fig. 3. Evolution of oxygen distribution along interface between CL and GDL at $\Delta P = 7$ mbar and $\eta = 0.2$ V (a) $\varepsilon_1 = 0.3$; (b) $\varepsilon_1 = 0.4$; (c) $\varepsilon_1 = 0.6$; (d) $\varepsilon_1 = 0.8$.

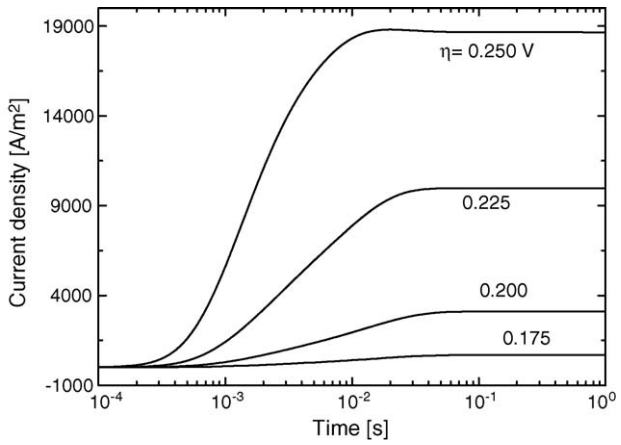

Fig. 4. Evolutions of average current density with various surface overpotentials η at $\Delta P = 7$ mbar and $\varepsilon_1 = 0.6$.

higher porosity of GDL leads to better cell performance at the only consideration of mass transport. The value of time constant is quite less, about 0.1 s, and is generally less than that of the PEM fuel cell with straight flow field [11].

As the catalyst layer is quite thin, the oxygen mass distribution in this layer can be regarded one-dimensional, and the distribution along the interface between the catalyst layer and the GDL can represents the distribution in whole CL region. Fig. 3 shows the evolutions of oxygen distributions along the interface between CL and GDL at $\Delta P = 7$ mbar and $\eta = 0.2$ V under different values of ε_1, 0.3, 0.4, 0.6 and 0.8. The time needed for almost reaching steady state from start-up condition can be figured out to be about 0.1 s. When the porosity is larger, uniformity of current distribution is better.

The evolutions of average current density with various surface overpotentials η under a certain pressure drop 7 mbar and porosity of GDL 0.6 are presented in Fig. 4. A careful inspection of Fig. 4 discloses that as the η increases, the average current density in steady state rises, and the time constant of start-up operation decreases. Additionally, the time constant varies largely, ranging from 0.01 to 0.1 s.

The evolutions of oxygen distribution along the interface between CL and GDL under different values of η, 0.175, 0.200, 0.225 and 0.250 V at constant pressure drop of 7 mbar and porosity of GDL 0.6 are shown in Fig. 5. It is clearly found in Fig. 5 that the times needed for almost reaching steady state from start-up for different surface overpotentials are very fast and range from 0.01 s to 0.1 s.

Figs. 6 and 7 compare the effects of pressure drop on the dynamical behaviors of the PEM fuel cells. These two figures depict that the steady-state average current density increases

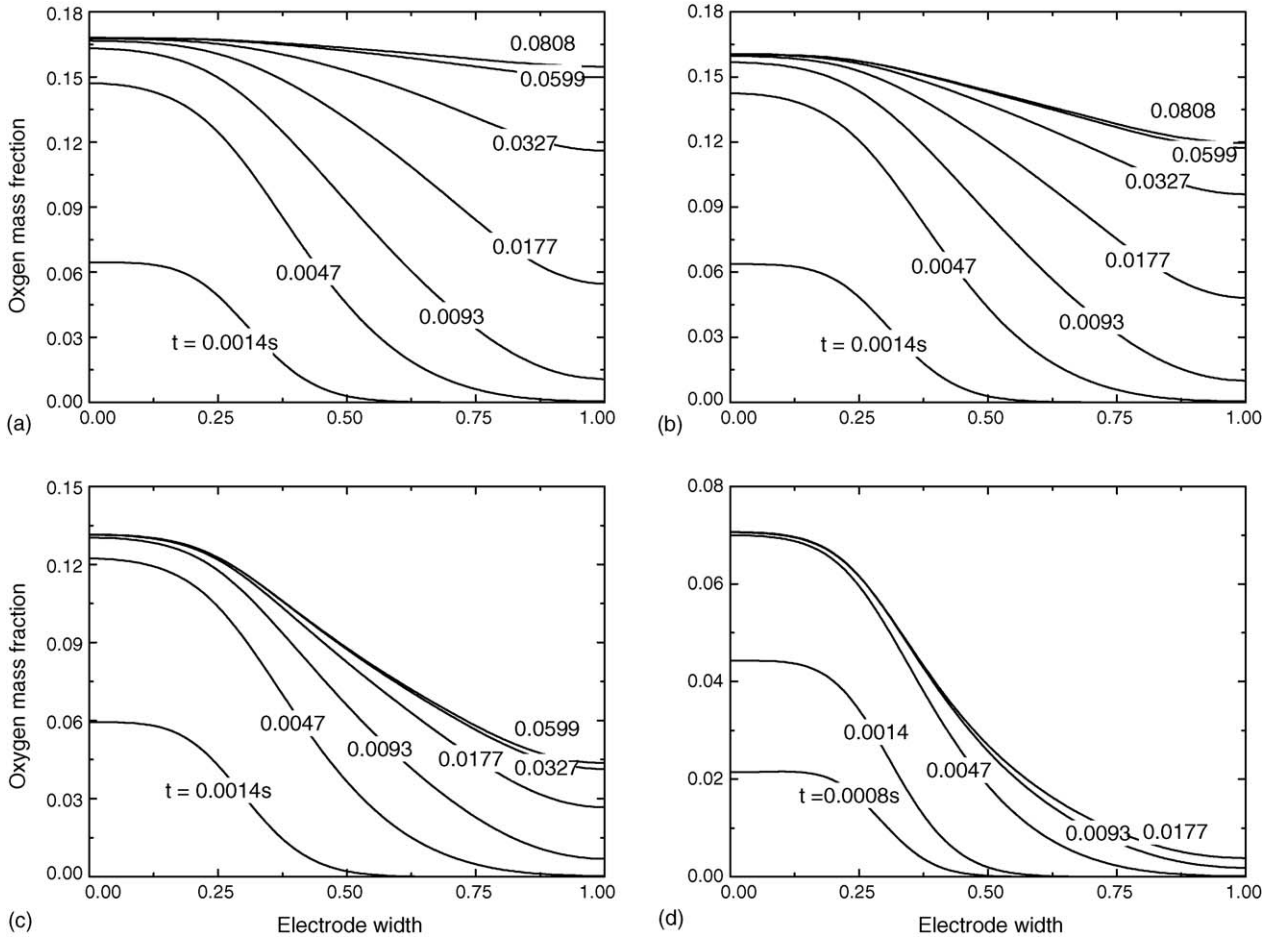

Fig. 5. Evolution of oxygen distribution along interface between CL and GDL at $\Delta P = 7$ mbar and $\varepsilon_1 = 0.3$ (a) $\eta = 0.175$ V; (b) $\eta = 0.200$ V; (c) $\eta = 0.225$ V; (d) $\eta = 0.250$ V.

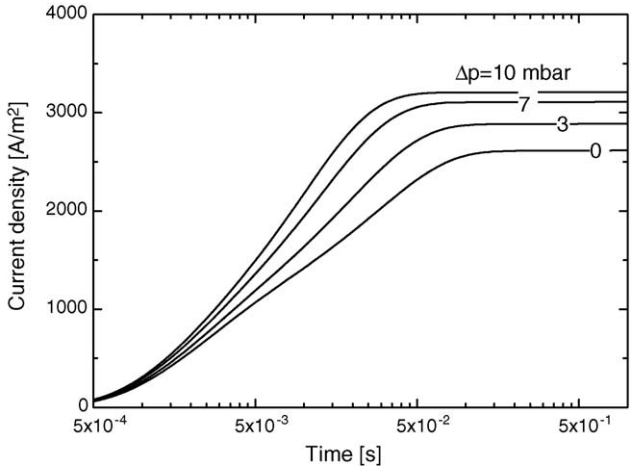

Fig. 6. Effects of pressure drop on the dynamical behaviors of the current density at $\eta = 0.20$ V and $\varepsilon_1 = 0.6$.

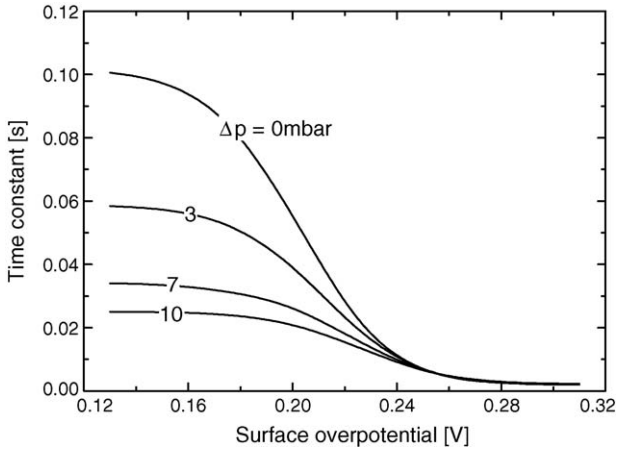

Fig. 8. Time constant variations with various pressure drops ΔP and surface overpotential at $\varepsilon_1 = 0.6$.

with the pressure drop and the response time decreases with pressure drop. The difference under various pressure drops, however, is smaller than that under various surface overpotentials.

Fig. 8 plots and compares the effects of the surface overpotential η and the pressure drop ΔP on the time constant t_c. Generally, the t_c decreases when the η increases or when ΔP increases, and the value of t_c is below 0.1 s. When the value of η is relatively small, the t_c changes dramatically with ΔP, and the value of t_c at $\Delta P = 0$ mbar is four times of that at $\Delta P = 10$ mbar. When the η is relatively large, for instance larger than 0.24 V, the t_c changes slightly, and remains a value below 0.02 s.

Although the initial oxygen mass fraction is zero, the distributions of oxygen change at once after the system is started up. The oxygen mass is always not uniformly distributed at the beginning. It is always true that the oxygen mass fraction near the inlet is larger than that near the outlet. The deviations between the oxygen mass fractions at different local spots vary with time, increasing firstly and then decreasing. When the η is relatively small, the oxygen mass distributions develop to be

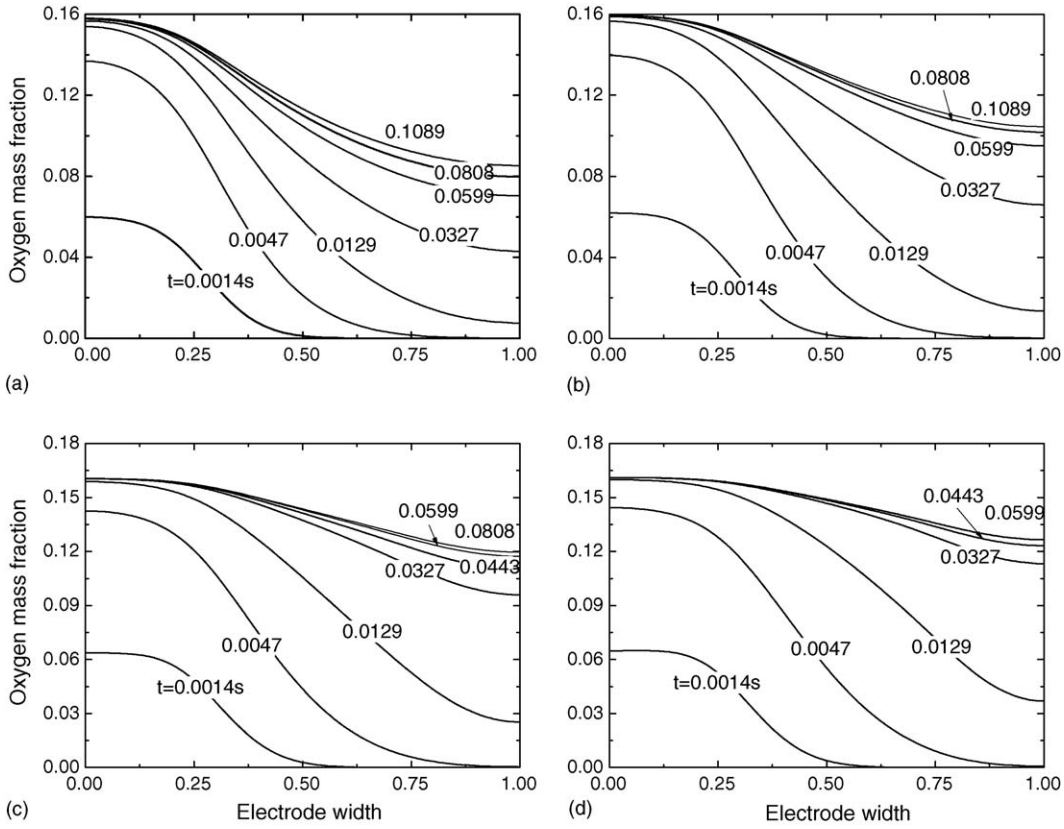

Fig. 7. Evolution of oxygen distribution along interface between CL and GDL at $\eta = 0.2$ V and $\varepsilon_1 = 0.6$ (a) $\Delta P = 0$ mbar; (b) $\Delta P = 3$ mbar; (c) $\Delta P = 7$ mbar; (d) $\Delta P = 10$ mbar.

Table 2
Corresponding current density and surface overpotential for four steady states

State no.	State 1	State 2	State 3	State 4
Current density (A/m^2)	4500	10000	15227	20430
Surface overpotential (V)	0.206888	0.22513	0.239513	0.256604

quite uniform. When the η is relatively large, the distributions are still non-uniform. It seems useful to introduce the ratio of ORR speed to gas transport speed to account for the discrepancy. The larger the value of the ratio is, the more non-uniform the distribution will be. In the corresponding conditions of Fig. 5, the pressure drop is constant, which means similar gas transport process, and η dominates ORR speed so as to dominate the ratio. In the corresponding conditions of Fig. 7, surface overpotential is constant, meaning similar ORR speed, and pressure drop dominates transport speed so as to dominate the ratio.

4.2. State-to-state operation

In the state-to-state operation, the initial conditions differ from that of start-up operation. The main feature is the oxygen mass distribution is not void but at a steady condition of the former state. In practical operation, operators change operating condition through external load adjustment, and the overpotential reflects the current drawn. So the current density, in this study, is chosen as the identification variant of various states. Stable cases analysis is firstly conducted. Fig. 9 shows the polarization curves for various pressure drops ΔP. It indicates that the limiting current density increases with the pressure drop. It is quite normal, as larger pressure drop means better gas transport capability and less transportation overpotential. Fig. 10 expresses the relation between surface overpotential and current density for various ΔP. According to the plot of Fig. 10, four states at $\Delta P = 7$ mbar are chosen to analyze transient characteristics of state-to-state operation. The detailed information about the four states is listed in Table 2.

Fig. 11 shows the dynamical performance from one state to another state. When the cell performance alters from a lower current density state to a higher current density state, as the upper graph depicts, the current density jumps up to a quite high level in the beginning, and then decreases gradually till to the steady state. On the contrary, when the cell performance alters from a higher current state to a lower state, as the lower graph depicts, the current density jumps down to a quite low level in the beginning, and then increase gradually. For both operations, the value of current density may change up to 5 times.

Table 3
Response time constants from state-to-state operation (Unit: s)

	start-up	State 1	State 2	State 3	State 4
start-up		0.024803	0.015634	0.00889	0.004333
State 1			0.016167	0.009272	0.004230
State 2		0.025046		0.009109	0.004084
State 3		0.024463	0.015564		0.003879
State 4		0.023891	0.015107	0.008432	

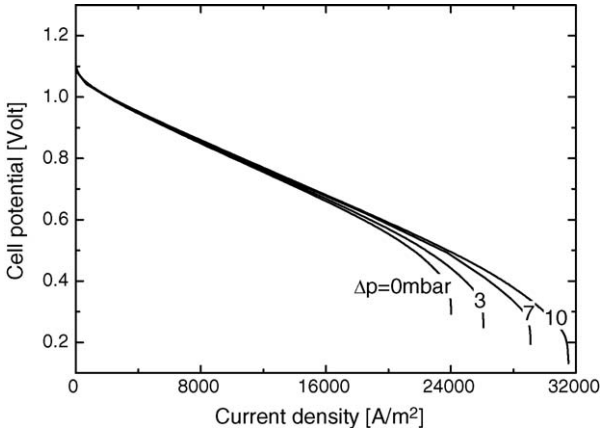

Fig. 9. The polarization curves for various pressure drops ΔP at $\varepsilon_1 = 0.6$.

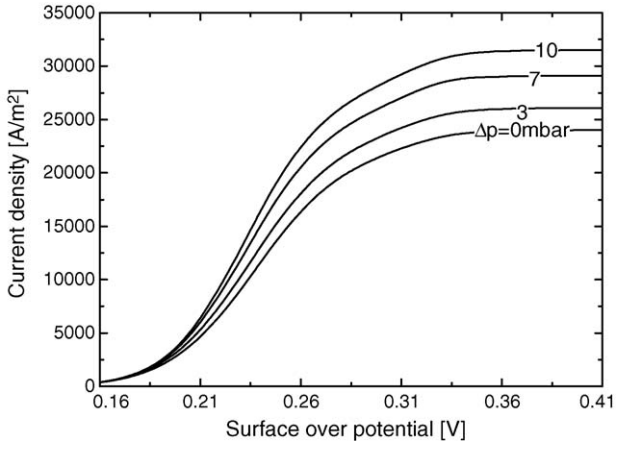

Fig. 10. Relation between current density and surface overpotential for various pressure drops ΔP.

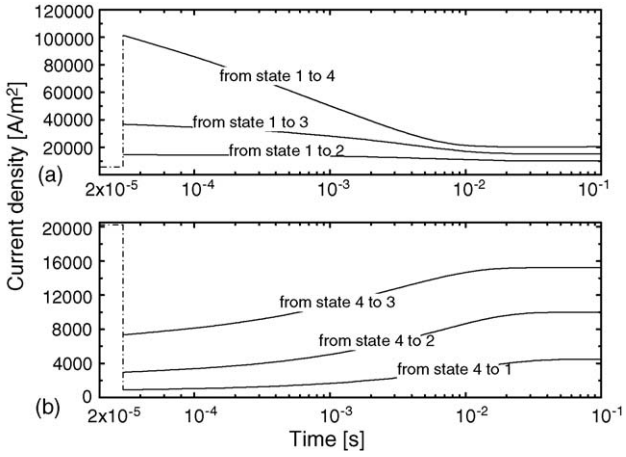

Fig. 11. Dynamic cell performance from one state to another state.

The time constants from one state to another state are listed in Table 3. The values of time constants also differ obviously. The large value is one order higher than the low one. As shown in Table 3, the response time generally depends on the new state. For instance, the response time is around 0.024 s when the new state is state 1. It is necessary to notice that the time constant from state A to state B is different with that from state B to state A. For example, the time constant t_c from state 1 to state 4 is 0.004230 s, and t_c from state 4 to state 1 is 0.023891 s.

5. Conclusions

In this work, the transient transport process of PEM fuel cell with interdigitated flow field is numerically investigated. Two operations, start-up and state-to-state, are analyzed. Parametric study is performed. Some conclusions are resulted.

1. The transient response time is generally quite small, below 0.1 s, and decreases with the surface overpotential, the porosity of GDL and the pressure drop. But when the surface overpotential is considerably large, the response time changes slightly with the pressure drop.
2. The ORR speed and mass transport speed determine the response time. Response time of the PEM fuel cell with interdigitated flow field is quite less than that of the PEM fuel cell with straight flow field, as the mass transport speed of the former cell is quite larger than that of the latter one. The mass transport of the former cell is dominated by both convection and diffusion, and that of the latter is only by diffusion.
3. The ratio of ORR speed to mass transport speed determines the steady oxygen mass distribution in catalyst layer. The larger the value of the ratio is, the more non-uniform the distribution will be. A relatively low overpotential, a high porosity of GDL or a high pressure drop leads to a better uniformity in current density distribution along the width of the cell.
4. For state-to-state operation, the value of current density changes largely, especially in the beginning. The response time mainly depends on the new state condition.

Acknowledgement

The study was supported by the National Science Council, the Republic of China, through the grants NSC 93-2212-E-211-011.

References

[1] D.N. Bernadi, M.W. Verbrugge, Mathematical model of a gas diffusion electrode bonded to a polymer electrolyte, AIChE J. 37 (8) (1991) 1151–1163.
[2] V. Guran, R. Barbir, H. Liu, J. Electrochem. Soc. 147 (2000) 2468–2477.
[3] T.E. Springer, T.A. Zawodzinski, S. Gottesfeld, J. Electrochem. Soc. 138 (1991) 2334.
[4] T. Okada, G. Xie, O. Gorseth, S. Kjelstrup, N. Nakamura, T. Arimura, Ion and water transport characteristics of Nafion membranes as electrolytes, Electrochim. Acta 43 (1998) 3741–3747.
[5] S. Dutta, S. Shimpalee, J.W. Van Zee, Int. J. Heat Mass Transfer 44 (2001) 2029–2042.
[6] L.R. Jordan, A.K. Shukla, T. Behrsing, N.R. Avery, B.C. Muddle, M. Forsyth, J. Appl. Electrochem. 30 (2000) 641–646.
[7] J.S. Yi, T.V. Nguyen, Multi-component transport in porous electrodes of proton exchange membrane fuel cells using the interdigitated gas distributors, J. Electrochem. Soc. 146 (1) (1999) 38–45.
[8] W. He, J.S. Yi, T.V. Nguyen, Two-phase flow model of the cathode of PEM fuel cells using interdigitated flow fields, AIChE J. 46 (10) (2000) 2053–2063.
[9] W.M. Yan, C.Y. Soong, F. Chen, H.S. Chu, Effects of flow distributor geometry and diffusion layer porosity on reactant gas transport and performance o f proton exchange membrane fuel cells, J. Power Sources 125 (2004) 27–39.
[10] F. Chen, Y.G. Su, C.Y. Soong, W.M. Yan, H.S. Chu, Transient behavior of water transport in the membrane of PEM fuel cell, J. Electroanal. Chem. 566 (2004) 85–93.
[11] W.M. Yan, C.Y. Soong, F. Chen, H.S. Chu, Transient behaviors of reactant gas transport and performance of PEM fuel cells, J. Power Sources 143 (2005) 48–56.
[12] Z.H. Wang, C.Y. Wang, K.S. Chen, Two-phase flow and transport in the air cathode of proton exchange membrane fuel cells, J. Power Sources 94 (2001) 40–50.
[13] P.C. Carman, Flow of gases through porous media, Academic Press, New York, 1965.
[14] K.H. Choi, D.H. Peck, C.S. Soo Kim, D.R. Shin, T.H. Lee, Water transport in polymer membranes for PEMFC, J. Power Sources 86 (2000) 197–201.
[15] J.S. Yi, T.V. Nguyen, An along-the-channel model for proton exchange membrane fuel cells, J. Electrochem. Soc. 145 (1998) 1149.
[16] D. Natarajan, T.V. Nguyen, A two-dimensional, two-phase, multicomponent, transient model for the cathode of a proton exchange membrane fuel cll using conventional gas distributors, J. Electrochem. Soc. 148 (2001) 1324–1335.
[17] Y. Wang, C.Y. Wang, Modeling polymer electrolyte fuel cells with large density and velocity changes, J. Electrochem. Soc. 152 (2) (2005) A445–A453.
[18] F.P. Incropera, D.P. Dewitt, Fundamentals of Heat and Mass Transfer, John Wiley & Sons, New York, 2002, p. 849.